Cite this paper as: *Dalton Trans*, **2018**, *47*, 859-867, DOI: 10.1039/C7DT04335J

Journal Name

ARTICLE

# Slow Relaxation of Magnetization in a Bis-*mer*-Tridentate Octahedral Co(II) Complex

Darunee Sertphon,[a]† Keith S. Murray,[b] Wasinee Phonsri,[b] Jesús Jover,[c] Eliseo Ruiz,[c] Shane G. Telfer,[d] Adil Alkaş,[d] Phimphaka Harding[a] and David J. Harding[a*]

Received 00th January 20xx,
Accepted 00th January 20xx

DOI: 10.1039/x0xx00000x

**www.rsc.org/**

Reaction of a rigid tridentate ligand *o*-[(1*H*-imidazol-2-yl)methylideneamino]phenol (2-$H_2$imap) with $Co(ClO_4)_2$ in the presence of $NaN_3$ or $Co(NO_3)_2$ without a base yields $[Co^{II}(2\text{-Himap})_2]$ **1** and $[Co^{III}(2\text{-Himap})_2]NO_3{\cdot}MeOH$ **2**, respectively. Both complexes exhibit a *mer*-octahedral geometry with the cobalt centre being distorted along an octahedral-trigonal prismatic pathway. The packing in **1** and **2** is dominated by H-bonding forming 2D sheets and 1D chains, respectively. Detailed *dc* and *ac* magnetic studies indicate that **1** is a field-induced single-ion magnet (SIM) with $D$ = 36.7 $cm^{-1}$, $E$ = 2.0 $cm^{-1}$ and $U_{eff}$ = 14 K. Extensive *ab initio* calculations support these conclusions and suggest that relaxation of the magnetization occurs principally through direct quantum tunnelling in the ground state, and a Raman process at higher temperatures. This contrasts with the recently reported series of *mer*-$[Co(L)_2]$ (L = monoanionic NNO donor ligand; *Inorg. Chem*., 2017, **56**, 6056–6066) complexes where $D$ is negative and highlights the importance of supramolecular interactions in subtly altering the coordination sphere thereby impacting the magnetic behaviour.

## Introduction

Single molecule magnets are compounds which exhibit slow relaxation of their magnetism of purely molecular origin.[1] They were first discovered in the 1990s and have been extensively investigated as they have a myriad of potential applications.[2–5] Much of the early work focused on metal clusters with the aim of increasing the total spin as the barrier to spin reversal ($U_{eff}$) depends directly on that term: $U_{eff} = |D| S^2$, where $S$ = the total spin of the complex and $D$ is the axial zero-field splitting (zfs) parameter; when $S$ is a half-integer $U_{eff} = |D|(S^2 - {}^1/_4)$. While this was successful to some degree many of these larger spin systems still exhibited low barriers due to very small $D$ values. In 2003, Ishikawa and co-workers discovered that the double decker complexes $[LnPc_2][NBu_4]$ (Ln = Tb, Dy) exhibit slow magnetic relaxation, with the Tb(III) complex having a barrier of 230 $cm^{-1}$.[6] These systems came to be known as single-ion magnets (SIMs)[7–9] and have driven much of the recent research in molecular magnetism. Indeed, very recently a Dy SIM was reported with an impressive blocking temperature of 60 K,[10,11] tantalizingly close to liquid nitrogen temperatures which could make high density data storage a reality with SIMs.

Prior to the advent of single molecule magnetism, cobalt(II) systems were some of the first complexes to be investigated for their ligand field splittings and spin-orbit coupling by Figgis *et al*.[12,13] and Gerloch *et al*.[14] These studies accounted not only for average susceptibility measurements on powders, but also explored single crystal anisotropy, generally measured at temperatures above 77 K by *dc* measurements. Cobalt(II) complexes remain interesting targets as SIMs due to the strong spin-orbit coupling of the metal ion that can, in combination with ligand field effects, lead to high magnetic anisotropy particularly in the orbitally degenerate $^4T_{1g}$ (parent) ground state octahedral species. The first Co(II) SIMs reported were distorted square pyramidal [{(2,6-*i*$Pr_2$-PhN=CR)$_2$py}Co(NCS)$_2$] complexes {R = Me, Ph} in which the Co(II) sitting above the basal plane is vital for observation of SMM behaviour.[15] Shortly afterwards, Long and coworkers reported the complex $[PPh_4]_2[Co(SPh)_4]$ that exhibits $D$ = −70 $cm^{-1}$ and $U_{eff}$ = 21 $cm^{-1}$.[16] This was the first Co(II) SIM to show slow relaxation of magnetization in zero field. Since then a range of tetrahedral systems has been explored and a very diverse range of $D$ values -5 to -160 $cm^{-1}$ and relaxation barriers (14-118 $cm^{-1}$) has been found. In general, these systems show that use of heavier donor atoms such as S, Se, P or I increases the magnetic anisotropy.[17–21] Geometry is also important, the tight bite angle of the ligand in the tetrahedral Co(II) SIM $[NHEt_3]_2[Co(pdms)]$ {pdms = 1,2-bis(methanesulfonamido)benzene} provides significant axial distortion at the Co(II) centre, leading to large magnetic anisotropy and a relatively high barrier of 118 $cm^{-1}$.[22] More recently, the linear system [(NHC)Co(NDmp)] (NHC = N-

[a] *Functional Materials and Nanotechnology Centre of Excellence, Walailak University, Thasala, Nakhon Si Thammarat, 80160, Thailand.*
[b] *School of Chemistry, Monash University, Clayton, Victoria, 3800, Australia.*
[c] *Departament de Química Inorgànica and Institut de Química Teòrica i Computacional, Universitat de Barcelona, Diagonal 645, E-08028 Barcelona, Spain.*
[d] *MacDiarmid Institute for Advanced Materials and Nanotechnology, Institute of Fundamental Sciences, Massey University, Palmerston North, New Zealand*
† Now at Department of Chemistry, Faculty of Science, 52/347Rangsit University, Phahonyothin Rd., Muang, Pathum Thani, 12000, Thailand
Electronic Supplementary Information (ESI) available: IR and NMR spectra, $\chi_M T$ vs. $T$ and $M$ vs. $H$ plots, and extra simulations are included in the ESI. See DOI: 10.1039/x0xx00000x

heterocyclic carbene; dmp = dimesitylphenyl), has been reported to have a relaxation barrier as high as 413 $cm^{-1}$; a new record in transition metal based SIMs.[23]

In contrast to tetrahedral Co(II) SIMs, octahedral systems are much rarer (Table 1), the first one was reported in 2012 by Cano, Pardo and coworkers.[24] Remarkably, in their *cis*-$[Co(dmphen)_2(NCS)_2]$ complex (dmphen = 2,9-dimethyl-1,10-phenanthroline) the value of *D* was positive (+98 $cm^{-1}$), implying that the slow relaxation observed is due to transverse, or easy plane (*xy*) anisotropy. Since then a number of other octahedral systems have been investigated and nearly all of them show positive *D* values, with the magnitude dependent on the ligands used, the degree of distortion and the *cis* or *trans* geometry adopted by the cobalt centre.[25–35] Nevertheless, the explanation for the occurrence of SMM behaviour, despite positive *D* parameters, is still not fully understood.[36] Moreover, in employing *mer*-directing ligands Powell *et al*. were able to reverse the sign of *D* as a result of distortion towards a trigonal prismatic geometry.[37] In trying to better understand the different factors which favour one relaxation mechanism over another in Co(II) SIMs we now report a Co(II) SIM, $[Co(2\text{-Himap})_2]$ **1**, with a rigid tridentate tight bite angle ligand.

**Table 1** Selected examples of octahedral Co(II) complexes with positive *D* values.

| Complex | *D* | $U_{eff}/K$ (H, Oe) | Ref. |
|---|---|---|---|
| *cis*-$[Co(dmphen)_2(NCS)_2]$ | +98 | 22.9 (2500) | 24 |
| $[Co(\mu\text{-L})(\mu\text{-OAc})Y(NO_3)_2]$ | +47 | 15.7 (1000) | 25 |
| $[Co(abpt)_2(tcm)]$ | +48 | 86.2 (3000) | 26 |
| $[Co(acac)_2(H_2O)_2]$ | +57 | 22.6 (various) | 36 |
| $[Co(9Accm)_2(py)_2]$ | +74 | Not given (500) | 27 |
| $[Co(9Accm)_2(bipy)]$ | +24 | Not given (700) | 27 |
| $[Co(bpy)_2(ClAn)]\cdot EtOH$ | +65.9 | 16.6 (600) | 28 |
| $NEt_4[Co(hfac)_3]$ | +118 | 19.5 (1000) | 29 |
| $[Co(pydm)_2][dnbz]_2$ | +44 | 39.0 (400) | 33 |
| $[Co(bzpy)_4X_2]$ | +106 (X = Cl) | | 34 |
| | +90.5 (X = NCS) | 27.7 (400) | |
| $[Co(dppm^{O,O})_3][CoBr_4]$ | +147 | Not given (4000) | 35 |

dmphen = 2,9-dimethyl-1,10-phenanthroline; L = *N*,*N*',*N*''-trimethyl-N,N''-bis(2-hydroxy-3-methoxy-5-methylbenzyl)diethylenetriamine; abpt = 4-amino-3,5-bis(2-pyridyl)-1,2,4-triazole; tcm = tricyanomethanide anion; 9Accm = 1,7-Bis(9-anthryl)-1,6-heptadiene-3,5-dionate; Cl-An = chloranilate; bzpy = 4-benzylpyridine; $dppm^{O,O}$ = bis(diphenyl-phosphanoxido)methane; pydm = 2,6-pyridinedimethanol; dnbz = 3,5-dinitrobenzoato; hfac = hexafluoroacetylacetonate.

## Results and Discussion

### Basic characterization and structural studies

The compound, $[Co(2\text{-Himap})_2]$ **1** was prepared by diffusion of a solution of $Co(ClO_4)_2$ into a solution of the ligand 2-$H_2$imap[38] with $NaN_3$ added as a base. The choice of cobalt starting material and base were found to be critical in isolating **1** with $Co(NO_3)_2$ yielding instead the Co(III) compound $[Co(2\text{-Himap})_2]NO_3\cdot MeOH$ **2**.

IR spectroscopic studies indicate a strong similarity between the compounds with the imine stretch at 1587 and 1579 $cm^{-1}$ for **1** and **2**, respectively (Figure S1). These values are a little lower than those previously reported by Sanmartín-Matalobos *et al*. in $[M(2\text{-Himap})_2M(2\text{-}H_2imap)_2]^{2+}$ (M = Ni, Cu; 1610-1614 $cm^{-1}$).[38] The nitrate band is visible only in **2** at 1384 $cm^{-1}$. $^1$H NMR spectroscopic studies of **2** in $d^6$-DMSO (Figure S2 in the ESI) show the typical sharp peaks of diamagnetic Co(III) in the aromatic region attributable to the 2-Himap ligand while the peak at 3.18 ppm is due to the MeOH that crystallizes in the lattice (*vide infra*).

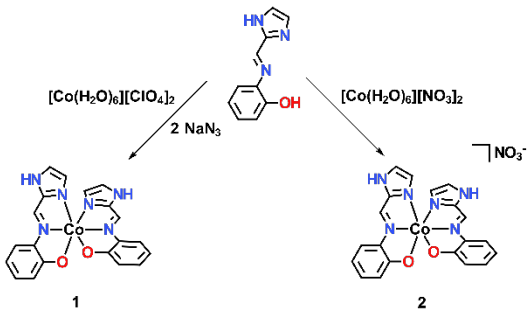


**Scheme 1** Synthesis of $[Co(2\text{-Himap})_2]$ **1** and $[Co(2\text{-Himap})_2]NO_3$ **2**.

**Table 2** Crystallographic data and structure refinement for **1** and **2**.

| | **1** | **2** |
|---|---|---|
| Formula | $C_{20}H_{16}CoN_6O_2$ | $C_{21}H_{20}CoN_7O_6$ |
| Molecular weight / $gmol^{-1}$ | 431.32 | 525.36 |
| Crystal system | Orthorhombic | Triclinic |
| Space group | *Pbcn* | $P\bar{1}$ |
| *1* | 11.8110(7) | 8.4486(5) |
| *b* / Å | 9.2017(5) | 10.2104(7) |
| *c* / Å | 17.5762(9) | 12.8436(9) |
| α / ° | 90.00 | 96.875(7) |
| β / ° | 90.00 | 98.442(7) |
| γ / ° | 90.00 | 101.045(7) |
| T / K | 296 | 123 |
| Cell volume / $Å^3$ | 1910.20(18) | 1063.09(13) |
| *Z* | 4 | 2 |
| Absorption coefficient/$mm^{-1}$ | 0.928 | 6.836 |
| Reflections collected | 6022 | 6524 |
| Independent reflections, $R_{int}$ | 1693, 0.062 | 2662, 0.0946 |
| Max. and min. transmission | 0.746, 0.685 | 1.00, 0.099 |
| Restraints/parameters | 0/136 | 43/317 |
| Final R indices [$I>2\sigma(I)$]: $R_1$, $wR_2$ | 0.0414, 0.1058 | 0.0934, 0.2337 |

Complex **1** crystallizes in the orthorhombic space group P*bcn*, while complex **2** crystallizes in the triclinic group $P\bar{1}$. The structures were determined at 296 and 123 K, for **1** and **2** respectively.

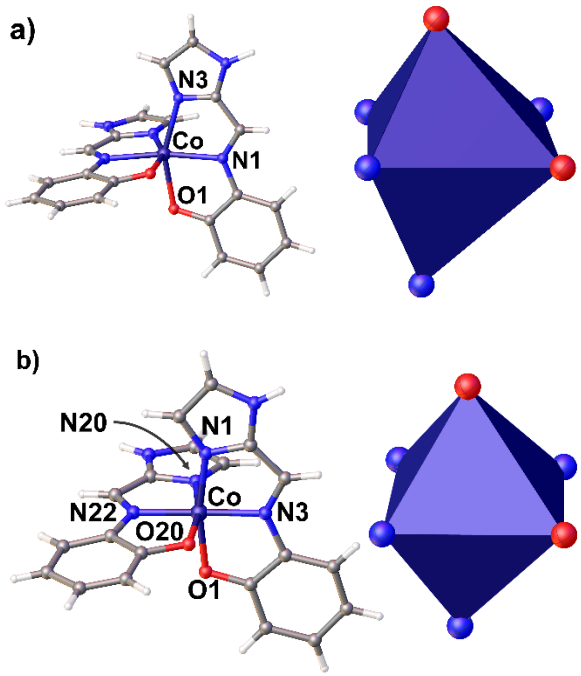


**Figure 1** View of the structures of a) **1** and b) **2** showing the key atom labels and the coordination polyhedra of the cobalt centres. Colour code: Co = purple, C = gray, N = blue, O = red.

Crystallographic data are given in Table 2 and the relevant Co-N/O bond lengths and angles are shown in Table 3. The Co-N/O bond lengths are typical for high spin Co(II) in **1**.[28] In contrast, the bond lengths in **2** are on average 0.166Å (Co-O) and 0.205 Å (Co-N) shorter than those in **1**, indicating that the metal centre is low spin Co(III). This is also confirmed by the octahedral distortion parameters[39,40] which show that **2** has a much more regular octahedral coordination (SHAPE[41] S-$O_h$ parameter for **2** = 0.74) environment than **1** (see Figure 1). The angle between the two ligands is almost 90° in both compounds and, in the case of **1**, is similar to that found in the related *mer*-[Co(L)$_2$] systems, (L = monoanionic NNO donor ligands based on 6-hydroxymethyl-pyridin-2-ylcarboxaldehyde) reported by the Powell group.[37] SHAPE analysis[41] shows that **1** is distorted along the octahedral-trigonal prismatic pathway but is closer to octahedral (3.25) than it is to trigonal prismatic geometry (9.50). This differs from *mer*-[Co(L)$_2$] where the geometry is much more ambiguous but closely mirrors the Co(II) centre in [Co(μ-L)(μ-OAc)Y(NO$_3$)$_2$].[25]

**Table 3** Selected bond lengths and octahedral distortion parameters (Å,°) for **1** and **2**.

| | **1** | **2** |
|---|---|---|
| Co1–O1 | 2.071(2) | 1.897(4) |
| Co1–O20 | - | 1.924(6) |
| Co1–N1 | 2.070(3) | 1.934(5) |
| Co1–N3 | 2.159(3) | 1.892(6) |
| Co1–N20 | | 1.950(7) |
| Co1–N22 | - | 1.885(6) |
| Co···Co | 7.4862(3) | 6.239(2) |
| | | 8.157(2) |
| $\Sigma^a$ | 103.4 | 49.3 |
| $\Theta^b$ | 321.4 | 165.3 |
| Plane-to-plane | 88.6 | 88.7 |

[a] $\Sigma = \sum_{i=1}^{12} |90 - \alpha_i|$, where $\alpha_i$ are the twelve cis N/O-Co-N/O angles.[39]

[b] $\Theta = \sum_{i=1}^{24} |60 - \theta_i|$, where $\theta_i$ are the 24 unique N/O-Co-N/O angles measured on the projection of two triangular faces of the octahedron along their common pseudo-threefold axis.[40]

The individual Co(II) centres in 1 are linked by strong N-H···O hydrogen bonds (N2···O1 = 2.641(4) Å, N2-H2···O1 = 170.0°) involving the imidazole N-H and a phenoxy oxygen atom. The H-bond donors and acceptors are arranged to give a 2D sheet (see Figure 2). An interesting feature of this structure is that the two [Co(2-Himap)2] enantiomers self-sort into strips, with only one enantiomer present in each strip. This differs from the previously reported [Cd(2-Himap)2] where the enantiomers are arranged into a 1D chain.42 This difference seems to be due to the greater distortion at the Cd centre that permits π-π interactions which support the N-H···O hydrogen bonds

Journal Name

ARTICLE

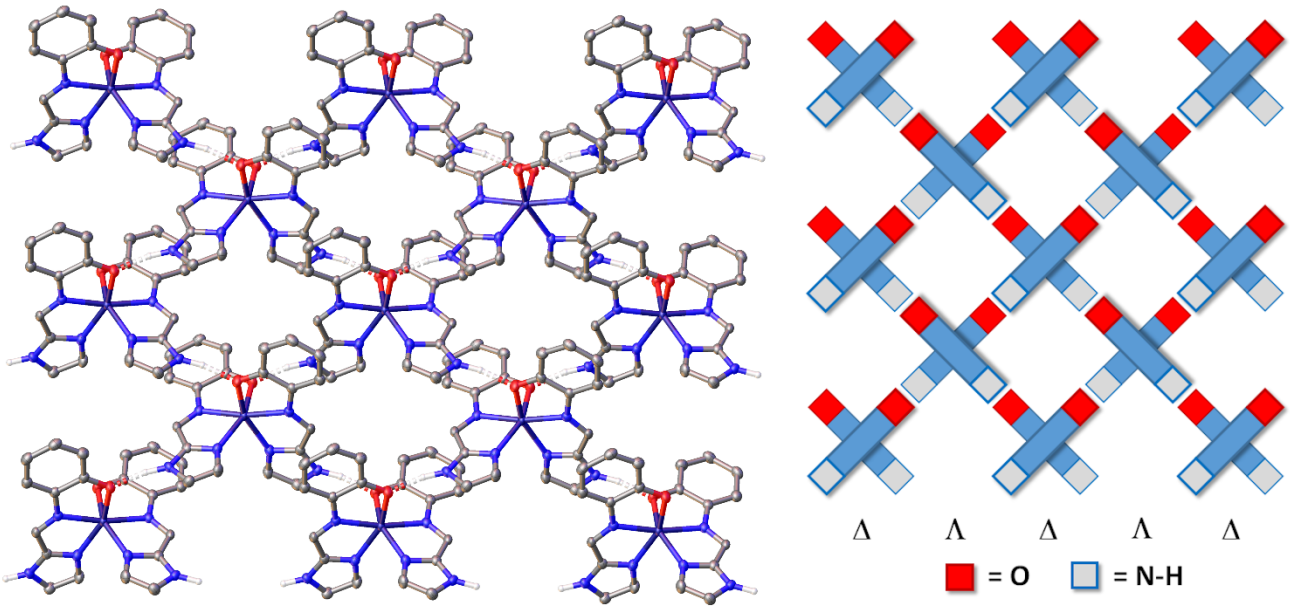


**Figure 2** View of the 2D H-bonding sheet in **1** (left) and a simplified representation of the packing motif (right).

The crystal packing of **2** is again dominated by hydrogen bonding this time between the nitrate counteranions, methanol molecules and the $[Co(2\text{-}Himap)_2]^+$ cations. In addition, there are now π-π interactions {plane-to-plane distance: 3.537(9) Å} which collectively link the $[Co(2\text{-}Himap)_2]^+$cations into a 1D chain (Figure 3). The 1D chains are then linked by C-H···O interactions involving the nitrate anion giving a strongly cooperative 3D supramolecular network.

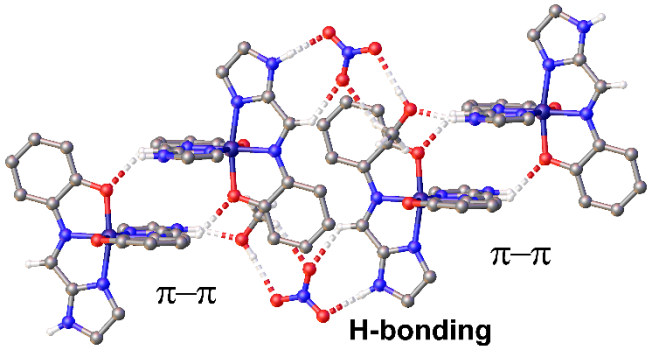


**Figure 3** View of the 1D chain formed by H-bonding and π-π interactions in **2**, for clarity selected H atoms have been removed.

**Magnetic properties of $[Co(2\text{-}Himap)_2]$**

Dc magnetic studies were undertaken on **1** between 2-300 K with applied fields of 0.1 T (2-70 K) and 1.0 T (2-300 K). These data are presented as $\chi_M T$ vs. $T$ and magnetization isotherm $M$ vs. $H$ plots in Figure S3 in the ESI. The $\chi_M T$ values are independent of the applied field indicating a lack of magnetic impurity or Zeeman level population effects. At 300 K, $\chi_M T$ = 2.40 $cm^3$ $mol^{-1}$ K and is significantly higher than the expected value of 1.875 $cm^3$ $mol^{-1}$ K for an isolated S = 3/2 Co(II) where g = 2.0. This indicates a considerable orbital angular momentum contribution as expected in a $^4T_{1g}$ system that exhibits magnetic anisotropy. The $\chi_M T$ value for **1** is similar to that reported in other octahedral Co(II) complexes where $\chi_M T$ is in the range 2.30-3.05 $cm^3$ $mol^{-1}$ K.[25–35] $\chi_M T$ values remain independent of temperature between 300 and ~100 K suggestive of a large distorted ligand field contribution, and spin-orbit coupling, which transform the $^4T_{1g}$ state into a lowest-energy $^4A_{2g}$ term (compressed tetragonal). Below 80 K $\chi_M T$ decreases rapidly reaching 1.30 $cm^3$ $mol^{-1}$ K at 2 K which is also indicative of ZFS of the $^4A_{2g}$ state, perhaps combined with remnant orbital degeneracy. The magnetization data reveal that the $M$ vs. $H$ curve at 2 K becomes almost saturated at higher fields with $M$ = 2.05 $N\beta$ at 2 K and 5 T. This is lower than the expected value for a S = 3/2 system where g > 2.0, probably because of spin-orbit coupling and magnetic anisotropy in **1**.

There are two approaches currently used to simultaneously fit the $\chi_M T$ vs. $T$ and $M$ vs $H$ plots. The first one assumes that

zero field splitting is dominant and uses the giant spin Hamiltonian approach to obtain $D$ (and $E$) and $g$ values.[37] The second approach uses the Figgis approach[12,13] that yields ligand field splitting and spin-orbit coupling values.[32,35] We have used the spin Hamiltonian, shown below, with a spin of 3/2, in the program PHI[43]

$$H = D(S_z^2 - [S(S+1)/3]) + E(S_x^2 - S_y^2) + \mu_B S \cdot g \cdot H \quad (1)$$

where $D$ is the axial zero field splitting (zfs) parameter; $E$ is the rhombic zfs, $\mu_B$ the Bohr magneton, $H$ is the applied dc field. The $g$ values were either kept isotropic or anisotropic, although the latter option is more appropriate for a Co(II) complex. The fits were very good for both the $\chi_M T$ vs. $T$ and the $M$ vs $H$ plots at temperatures of 2, 3, 4 and 5.5 K; Figure 4. The parameters obtained from the fits are: $D$ = +36.7 cm$^{-1}$; $E$ = 2.0 cm$^{-1}$; $g$ = 2.11, 2.48, 2.12. The use of a negative $D$ value gave unrealistic values of $E$, and thus this possibility can be discarded.

To better understand and quantify the magnetic anisotropy in **1** we undertook *ab initio* calculations using a multireference methodology; the computed second-order anisotropy parameters and excitation energies are collected in Table 4 ($\chi_M T$ vs. $T$ and $M$ vs. $H$ plots from the simulations are shown in Figures S4-5 in the ESI).

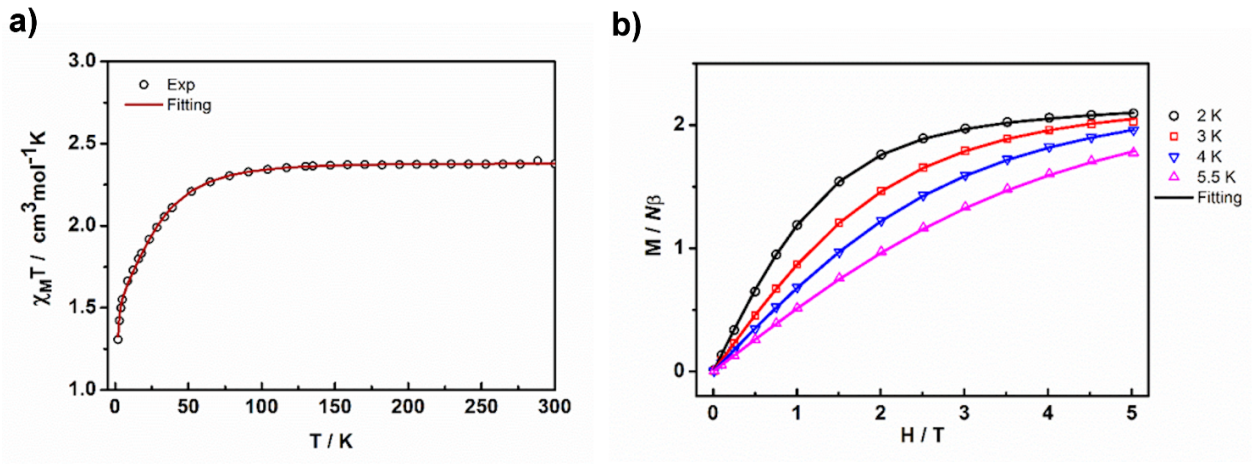


**Figure 4** Best fits of a) $\chi_M T$ vs $T$ in field of 1 T and of b) $M$ vs $H$ isotherms using the ZFS Hamiltonian in program PHI[43] with the parameter set given in equation 1.

**Table 4** ORCA/CASSCF, ORCA/CASSCF + NEVPT2, and MOLCAS/CASSCF + RASSI computed $D$, $|E|$, and g-values for the ground state of **1**. δ and Δ are the computed first excitation energies before and after including the spin-orbit effects, respectively. The Δ-value corresponds to the energy difference between the ground and the first excited Kramers' doublets.

| Method | $D_{calc}$ (cm$^{-1}$) | $\|E\|_{calc}$ (cm$^{-1}$) | δ (cm$^{-1}$) | Δ (cm$^{-1}$) | $g_{xx}$, $g_{yy}$, $g_{zz}$ |
|---|---|---|---|---|---|
| ORCA/CASSCF | 50.4 | 3.1 | 1339.8 | 101.3 | 2.03, 2.45, 2.53 |
| ORCA/NEVPT2 | 39.3 | 1.8 | 1919.8 | 78.8 | 2.03, 2.36, 2.41 |
| MOLCAS/CASSCF | 48.2 | 2.8 | 1439.9 | 96.8 | 2.03, 2.45, 2.51 |

These values have been obtained from two different electronic structure calculations using the ORCA[44] and MOLCAS[45–47] software packages. ORCA produces two sets of results: CASSCF and CASSCF + NEVPT2 (which introduces the dynamic correlation effects), both including spin-orbit contributions. MOLCAS has been employed to provide CASSCF results, including spin-orbit effects that have been introduced with the SO-RASSI method. Positive, and similar, D values are found with the three methods, as expected for an octahedral Co(II) complex.[46] The best agreement with the experimental data is found with the ORCA/NEVPT2 calculation: $D$ = 39.3 cm$^{-1}$ and $E$ = 1.8 cm$^{-1}$. In all cases, a 3/2 ground state is found before including spin-orbit effects. Under these conditions, the calculations show the existence of relatively low-lying spin-orbit free excited states (δ in Table 4) with energies around 1000-2000 cm$^{-1}$ above the ground state, which may be responsible of the observed anisotropy. This is also confirmed by the anisotropic g-values for the ground state. Once spin-orbit effects are included a set of Kramers' doublets (KDs, Δ) is obtained; the three methods again produce very similar results, indicating a low-lying KD around 100 cm$^{-1}$ above the ground state, which may participate in the spin relaxation processes (see below). The second KD is located at higher energies in all cases (1200-1800 cm$^{-1}$) and would not be expected to participate in the spin relaxation mechanism.

The sign and value of the $D$ parameter can be rationalized using the spin-orbit operator, which couples the ground and excited states. When the excited state results from the

excitation between orbitals with the same $|m_l|$ values, the $M_S$ = ±3/2 components are stabilized and a negative contribution to *D* is obtained. However, an excitation between orbitals involving a $|\Delta m_l|$ = 1 change, *i.e.* stabilizing the $M_S$ = ±1/2 components, leads to a positive contribution to the *D* value.[48] **1** displays a distorted octahedral core, which produces the d-orbital splitting shown in Figure 5. This orbital arrangement is obtained with the ORCA/CASSCF + NEVPT2 calculation by using the *ab initio* ligand field theory (AILF)[49,50] method. We find that the degeneracy of the $t_{2g}$ and $e_g$ orbitals of the regular octahedron is broken in **1**, indicating the transformation of the initial octahedral $^4T_{1g}$ ground state into a lowest-energy $^4A_{2g}$ term, and one of the former clearly moves up in energy (1573.4 $cm^{-1}$), far from the last doubly occupied orbital (83.9 $cm^{-1}$). The AILF method allows the identification of these orbitals; the last doubly occupied orbital is $d_{yz}$ (or $d_{xz}$, because these cannot be distinguished) while the first half-occupied orbital is $d_{xy}$; since these orbitals have a different $|m_l|$ value *i.e.* ±1 and ±2, respectively, the *D* value should be positive. This contrasts with the similar *mer*-[Co(L)$_2$] compounds which show negative *D* values.[37] The difference between the two systems is probably due to the greater distortion towards a trigonal prismatic geometry in *mer*-[Co(L)$_2$] when compared with **1**, and seems to be caused by H-bonding involving uncoordinated hydroxyl groups on the ligands.[37]

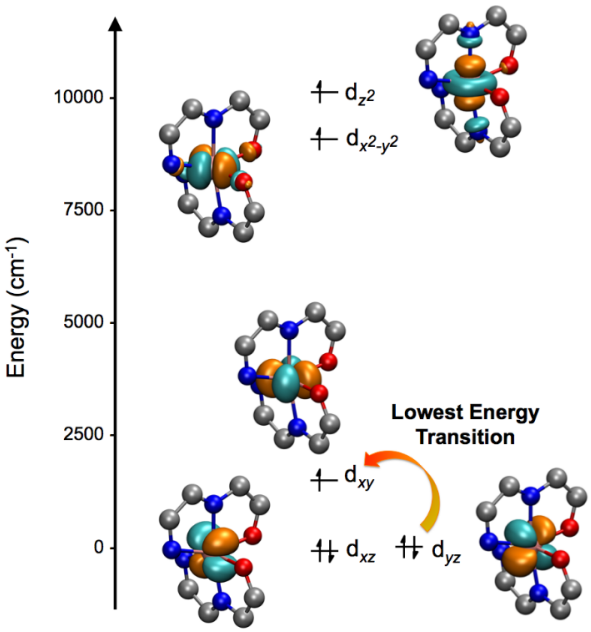


**Figure 5** AILF computed d-orbital splitting for **1** (orbital energies: $d_{xz}$ 0.0 $cm^{-1}$, $d_{yz}$ 83.9 $cm^{-1}$, $d_{xy}$ 1573.4 $cm^{-1}$, $d_{x2-y2}$ 9066.1 $cm^{-1}$, $d_{z2}$ 10150.2 $cm^{-1}$). Colour code: Co = pink, C = gray, N = blue, O = red; H atoms and parts of the 2-Himap ligand have been omitted for clarity.

The dynamics of magnetization were investigated using *ac*-magnetic measurements. The data were recorded with an applied field of 0.2 T between 2-9 K and 50-1488 Hz (Figure 6a). Under these conditions the out-of-phase magnetization shows a clear peak at higher frequencies, the signature of a single molecule magnet. As with many Co(II) SIMs at zero applied *dc* field there are no signals in the out-of-phase magnetization probably due to efficient quantum tunneling and consistent with the calculations below.

The program CC-FIT [CC-FIT Copyright 2014, Nicholas F. Chilton] was used to fit the Cole plots (Figure 6b) that showed semicircles at the lowest temperatures. The α values are 0.24 (1.8 K) to 0.07 (6 K) indicative of deviations from the Debye model and a range of distributions of the relevant relaxation processes. Usually, four mechanisms as shown in equation 2 are considered, direct, quantum tunneling, Raman and Orbach:

$$\tau^{-1} = AH^4T + \frac{B_1}{1+B_2H^2} + CT^n + \tau_0^{-1}\exp\left(\frac{-U_{eff}}{kT}\right) \qquad (2)$$

A common initial approach is to analyse the temperature dependence of the relaxation time $\tau$ values by plotting ln($\tau$) against 1/T (see ESI, Figure S6). The best fit for **1** using only an Orbach term gives a $U_{eff}$ value of 14 K. However, the calculated *D* value is 39.3 $cm^{-1}$ giving a 2D barrier of 78.6 $cm^{-1}$, considerably higher than the fitted barrier height.

Journal Name

ARTICLE

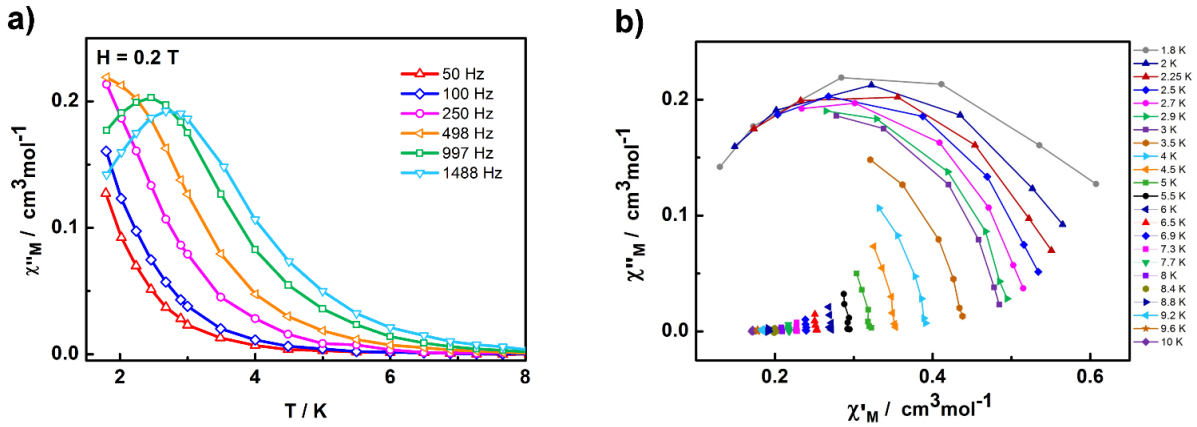


**Figure 6** a) Variable-frequency out-of-phase components of the *ac* magnetic susceptibility and b) Cole-Cole plot of **1** the solid lines being best fit.

This indicates that the thermal Orbach mechanism is not the main contributor to the temperature dependence.[24,37,51] The explanation for the occurrence of slow spin relaxation with positive *D* values has been explained by a combination of a principal direct mechanism (due to the presence of very effective hyperfine coupling in an I = 7/2 Co(II) system), a Raman mechanism and a strong nuclear spin-phonon interaction which must also be taken into account.[36]

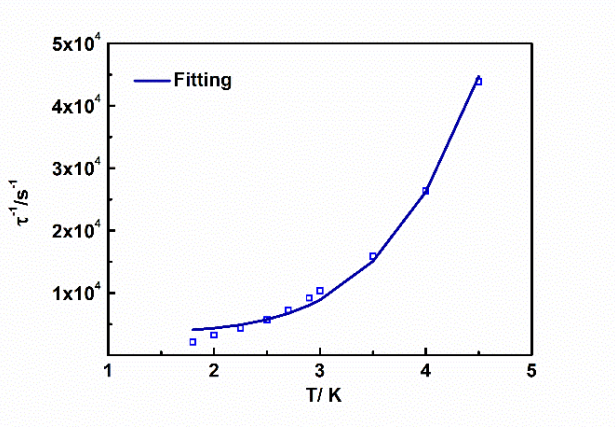


**Figure 7** Relaxation time vs. *T* plot and best fit as described using Eqn. 3 for **1** using *ac* $\chi_M''$ data in a *dc* field of 0.2 T.

In such a scenario, the temperature dependence of the spin relaxation time (see Figure 7) can be described by a Raman term and a field-dependent mechanism contribution $\tau_{FDM}^{-1}$

$$\tau^{-1} = \tau_{FDM}^{-1} + CT^n \quad (3)$$

the best fit for **1** is with $C$ = 19.12 $s^{-1}$ $K^{-5.10}$, $n$ = 5.10 and $\tau_{FDM}^{-1}$ 3685.1 $s^{-1}$. Although, $n$ is smaller than the hypothetical $n$ = 9 for a Kramers ion, the value is very similar to that reported for other easy-plane Co(II) complexes.[52] Interestingly, despite the differences in the sign of *D*, $U_{eff}$ is comparable with the values reported by Powell *et al*. for their *mer*-$[Co(L)_2]$ complexes.[37]

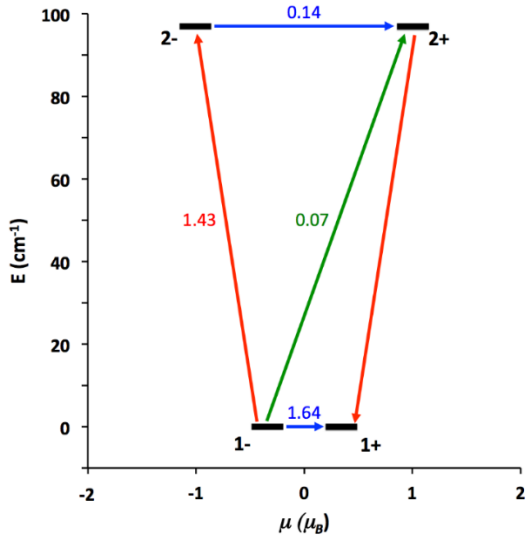


**Figure 8** Lowest two Kramers' doublets and *ab initio* computed relaxation mechanism in **1**. The thick black lines imply KDs as a function of their magnetic moment along the main anisotropy axis. Red lines indicate the magnetization reversal mechanism. The blue lines correspond to ground state QTM and thermally assisted-QTM via the first excited KD, and green and purple lines show the possible Orbach relaxation process. The values close to the arrows indicate

the matrix elements of the transition magnetic moments (above 0.1 an efficient spin relaxation mechanism is expected).

The computed relative energies of the lowest-lying KDs and the spin relaxation pathways of **1**, obtained with the MOLCAS/CASSCF + RASSI calculation, are shown in Figure 8. The spin relaxation mechanisms show a plausible pathway *via* direct quantum tunneling (QTM) in the ground state. The matrix elements of the transition magnetic moments found between states 1- and 1+ is 1.64, much higher than the required value of 0.1 associated with an efficient relaxation mechanism. The second KD may also be accessible (96.8 $cm^{-1}$) and should able to participate in alternative relaxation pathways, most probably through thermally assisted-QTM although the Orbach process is also possible. However, the $U_{eff}$ barrier obtained from the fit of the relaxation time (14 K) is much lower than these thermally-activated processes (139 K), and confirms the above fit that there is a significant Raman component to the relaxation mechanism.

## Conclusions

In summary we have prepared a new Co(II) field-induced SIM featuring a rare meridional geometry. The compound shows a distorted octahedral centre and strong magnetic anisotropy. Subtle differences between **1** and similar systems previously reported result in a positive value for *D* but a comparable relaxation barrier. The difference in the sign of *D* seems to be due distortion of the coordination sphere in *mer*-$[Co(L)_2]$ caused by H-bonding interactions and re-emphasizes the importance of supramolecular interactions in controlling not only the magnitude but the sign of *D*. In common with many octahedral Co(II) compounds direct and Raman processes are the dominant relaxation mechanisms. With more flexible ligands and/or different donor sets a more complete picture of the magnetostructural correlations should be forthcoming and efforts along these lines are currently being explored.

## Experimental

### General remarks

2-$H_2$imap was prepared as previously reported.[38] All other chemicals were purchased from Sigma-Aldrich and used as received. All reactions were performed in air with reagent grade solvents. IR data were measured on a Cary 630 Agilent Technologies IR spectrometer fitted with a Specac Golden Gate diamond ATR. $^1$H NMR spectra were collected on a Bruker 300 MHz spectrometer in $d^6$-DMSO at 298 K. Elemental analyses were carried out on a Eurovector EA3000 analyser by staff of the School of Chemistry, University of Bristol, UK. ESI-MS were carried out on a Bruker Daltonics 7.0T Apex 4 FTICR Mass Spectrometer by staff at the National University of Singapore.

### Synthesis of $[Co(2\text{-Himap})_2]$ 1

A solution of 2-$H_2$imap (0.109 g, 0.5 mmol) in $H_2O$ (3 $cm^3$) with $NaN_3$ (0.065 g, 1.0 mmol) was layered at the bottom of a test tube and then blank MeOH:$H_2O$ (1:1, 10 mL) was layered in the middle as a buffer layer. Finally, a solution of $[Co(H_2O)_6][ClO_4]_2$ (0.183 g, 0.5 mmol) in MeOH (5 $cm^3$) was layered on top and the test tube sealed. The solution was left for 2 weeks at room temperature, and red brown crystals were obtained at the buffer layer. The red brown crystals were isolated, washed with diethyl ether (2×2 $cm^3$) and air dried, yield 0.065 g (30%). m/z (ESI) 429 $[Co(2\text{-Himap})_2]^+$. $\nu_{max}$ (ATR)/$cm^{-1}$ 1587, 1461, 1384, 1249, 841, 747. Anal. Calc. for $1{\cdot}H_2O$ $C_{20}H_{18}N_6O_3Co$: C 53.47; H 4.04; N 18.70. Found: C 53.69; H 3.82; N 19.36%.

### Synthesis of $[Co(2\text{-Himap})_2]NO_3{\cdot}MeOH$ 2

2-Himap (0.437 g, 2mmol) was dissolved in MeOH (7 $cm^3$) and $[Co(H_2O)_6][NO_3]_2$(0.291 g, 1.0 mmol) in MeOH (5 $cm^3$) added dropwise into the ligand solution. The solution immediately turned deep red with a small amount of dark solid produced. After stirring for 15 minutes the solution was filtered into a test tube and left overnight at room temperature, giving dark crystals. The crystals were isolated by filtration, washed with diethyl ether (2×2 $cm^3$) and air dried, yield 0.331 g (61%). $\nu_{max}$ (ATR)/$cm^{-1}$ 3119, 3060, 1579, 1547, 1432, 1310, 1255, 1122, 743. *m/z* (ESI) 429 $[Co(2\text{-Himap})_2]^+$. Anal. Calc. for $C_{21}H_{20}N_7O_6Co$: C, 48.02; H, 3.84; N, 18.66. Found: C, 47.80; H, 3.86; N, 18.63%.

### X-ray crystallography

Crystals of **1** and **2** were mounted on a glass fibre using perfluoropolyether oil and in the case of **2** cooled rapidly to 123 K in a stream of cold nitrogen. The diffraction data of **1** were collected on a Bruker APEXII area detector with graphite monochromated MoKα (λ = 0.71073 Å).[53] After data collection an empirical absorption correction (SADABS) was applied.[54] In the case of **2**, data were collected at 123 K on a Rigaku Spider diffractometer equipped with a MicroMax MM007 rotating anode generator, Cu$_{\alpha}$ radiation (λ = 1.54178 Å), high-flux Osmic multilayer mirror optics, and a curved image-plate detector.[55] The data were integrated and scaled and averaged with FS Process. The structures were then solved by direct methods and refined on all $F^2$ data using the SHELX suite of programs or Olex2.[56–58] In all cases non-hydrogen atoms were refined with anisotropic thermal parameters; hydrogen atoms were included in calculated positions and refined with isotropic thermal parameters which were *ca*. 1.2 × (aromatic CH) or 1.5 × (Me, OH) the equivalent isotropic thermal parameters of their parent carbon atoms. Crystallographic data and structure refinement parameters are given in Table 2. All pictures were generated using OLEX2.[59] The CCDC numbers for the X-ray crystallographic data presented in this paper are 1585230 and 1585229 for **1** and **2**, respectively.

### Magnetic measurements

Data were collected using a Quantum Design MPMS 7 SQUID magnetometer under applied fields of 0.1 T (2-70 K) and 1.0 T (2-300 K). The crystalline sample was placed in a gel capsule for all data collection. Magnetization isotherms were collected

 

at 2, 3, 4, 5.5, 10 and 20 K between 0-5 T. Alternating current susceptibility measurements were undertaken in an applied field of 0.2 T between 2-9 K and 50-1488 Hz. All data were corrected for the sample holder and diamagnetic contributions.

**Quantum Chemical Calculations**

The calculation of the second-order magnetic anisotropy (or zero-field splitting) parameters (*D* and *E*) has been carried out with two different software packages: MOLCAS 8.0[45–47] and ORCA.[44] We have employed MOLCAS (along with the SINGLE_ANISO[60,61] code) to carry out a CASSCF calculation of the energy states of the Co(II) complex. After that, the spin-orbit coupling has been introduced, as implemented in the SO-RASSI (Restricted Active Space State Interaction) approach, to mix up these energies and obtaining the final energy states. In these calculations we have employed an all electron ANO-RCC basis set:[62–65] Co atoms (6s5p4d2f), N (4s3p2d1f), O (4s3p2d1f), C (3s2p) and H (2s).

A CASSCF calculation was also carried out with ORCA; the dynamic correlation effects were included through the n-electron valence state perturbation theory NEVPT2[66–68] method. In all cases the spin–orbit effects were included using the quasi-degenerate perturbation theory (QDPT) and the magnetic anisotropy parameters were obtained using the effective Hamiltonian method. In these calculations all the atoms are described by the def2-TZVPP basis set,[69,70] including the corresponding auxiliary basis sets for correlation and Coulomb fitting. In both sets of calculations, the active space is formed by the seven d electrons of the Co(II) centre and the 5d orbitals (7,5); and all the quadruplet (10) and doublet (40) states have been taken into account.

## Conflicts of interest

There are no conflicts to declare.

## Acknowledgements

We gratefully acknowledge the Thailand Research Fund (RSA5880048) for funding this research and financial support from the Thailand Research Fund in the form of a Royal Golden Jubilee scholarship to D. S. (PHD/0135/2554). K.S.M. thanks the Australian Research Council for a Discovery grant. The research reported here was also supported by the Spanish *Ministerio de Economía y Competitividad* (grant CTQ2015-64579-C3-1-P, MINECO/FEDER, UE). E.R. thanks Generalitat de Catalunya for an ICREA Academia award. J.J. and E.R. thankfully acknowledge the computer resources in the Consorci Serveis Universitaris de Catalunya (CSUC). Declan Wain is thanked for curve fitting. Ivana Borilović is thanked for help with the latest version of Program PHI and Boujemaa Moubaraki is thanked for magnetic measurements.

## Notes and references

1 D. Gatteschi, R. Sessoli and J. Villain, *Molecular Nanomagnets*, Oxford University Press, 2006.
2 R. Sessoli, D. Gatteschi, A. Caneschi and M. A. Novak, *Nature*, 1993, **365**, 141–143.
3 G. Christou, D. Gatteschi, D. N. Hendrickson and R. Sessoli, *MRS Bull.*, 2000, 66–71.
4 R. E. P. Winpenny, *Angew. Chem. Int. Ed.*, 2008, **47**, 7992–4.
5 G. A. Timco, T. B. Faust, F. Tuna and R. E. P. Winpenny, *Chem. Soc. Rev.*, 2011, **40**, 3067.
6 N. Ishikawa, M. Sugita, T. Ishikawa, S. Y. Koshihara and Y. Kaizu, *J. Am. Chem. Soc.*, 2003, **125**, 8694–8695.
7 G. A. Craig and M. Murrie, *Chem. Soc. Rev.*, 2015, **44**, 2135–2147.
8 S. Gómez-Coca, D. Aravena, R. Morales and E. Ruiz, *Coord. Chem. Rev.*, 2015, **289–290**, 379–392.
9 J. M. Frost, K. L. M. Harriman and M. Murugesu, *Chem. Sci.*, 2016, **6**, 1–22.
10 C. A. P. Goodwin, F. Ortu, D. Reta, N. F. Chilton and D. P. Mills, *Nature*, 2017, **548**, 439–442.
11 F.-S. Guo, B. M. Day, Y.-C. Chen, M.-L. Tong, A. Mansikkamäki and R. A. Layfield, *Angew. Chemie Int. Ed.*, 2017, **56**, 11445–11449.
12 B. N. Figgis, *Introduction to ligand fields*, Wiley-VCH, New York, 1966.
13 B. N. Figgis, M. Gerloch, J. Lewis, F. E. Mabbs and G. A. Webb, *J. Chem. Soc. A Inorganic, Phys. Theor.*, 1968, 2086.
14 R. B. Bentley, M. Gerloch, J. Lewis and P. N. Quested, *J. Chem. Soc. A*, 1971, 3751–3756.
15 T. Jurca, A. Farghal, P. H. Lin, I. Korobkov, M. Murugesu and D. S. Richeson, *J. Am. Chem. Soc.*, 2011, **133**, 15814–15817.
16 J. M. Zadrozny and J. R. Long, *J. Am. Chem. Soc.*, 2011, **133**, 20732–20734.
17 M. R. Saber and K. R. Dunbar, *Chem. Commun.*, 2014, **50**, 12266–12269.
18 L. Smolko, J. Černák, M. Dušek, J. Miklovič, J. Titiš and R. Boča, *Dalton Trans.*, 2015, **44**, 17565–17571.
19 S. Vaidya, A. Upadhyay, S. K. Singh, T. Gupta, S. Tewary, S. K. Langley, J. P. S. Walsh, K. S. Murray, G. Rajaraman and M. Shanmugam, *Chem. Commun.*, 2015, **51**, 3739–3742.
20 S. Vaidya, S. K. Singh, P. Shukla, K. Ansari, G. Rajaraman and M. Shanmugam, *Chem. - A Eur. J.*, 2017, **23**, 9546–9559.
21 J. M. Zadrozny, J. Telser and J. R. Long, *Polyhedron*, 2013, **64**, 209–217.
22 Y. Rechkemmer, F. D. Breitgoff, M. van der Meer, M. Atanasov, M. Hakl, M. Orlita, P. Neugebauer, F. Neese, B. Sarkar and J. van Slageren, *Nat. Commun.*, 2016, **7**, 10467.
23 X.-N. Yao, J.-Z. Du, Y.-Q. Zhang, X.-B. Leng, M.-W. Yang, S.-D. Jiang, Z.-X. Wang, Z.-W. Ouyang, L. Deng, B.-W. Wang and S. Gao, *J. Am. Chem. Soc.*, 2017, **139**, 373–380.
24 J. Vallejo, I. Castro, R. Ruiz-García, J. Cano, M. Julve, F. Lloret, G. De Munno, W. Wernsdorfer and E. Pardo, *J. Am. Chem. Soc.*, 2012, **134**, 15704–15707.
25 E. Colacio, J. Ruiz, E. Ruiz, E. Cremades, J. Krzystek, S. Carretta, J. Cano, T. Guidi, W. Wernsdorfer and E. K. Brechin, *Angew. Chemie - Int. Ed.*, 2013, **52**, 9130–9134.
26 R. Herchel, L. Váhovská, I. Potočňák and Z. Trávníček, *Inorg. Chem.*, 2014, **53**, 5896–5898.
27 R. Díaz-Torres, M. Menelaou, O. Roubeau, A. Sorrenti, G. Brandariz-de-Pedro, E. C. Sañudo, S. J. Teat, J. Fraxedas, E. Ruiz and N. Aliaga-Alcalde, *Chem. Sci.*, 2016, **7**, 2793–2803.
28 R. Ishikawa, Y. Horii, R. Nakanishi, S. Ueno, B. K. Breedlove, M. Yamashita and S. Kawata, *Eur. J. Inorg. Chem.*, 2016, **2016**,

3220.
29 A. V. Palii, D. V. Korchagin, E. A. Yureva, A. V. Akimov, E. Y. Misochko, G. V. Shilov, A. D. Talantsev, R. B. Morgunov, S. M. Aldoshin and B. S. Tsukerblat, *Inorg. Chem.*, 2016, **55**, 9696−9706.
30 S. Vaidya, S. Tewary, S. K. Singh, S. K. Langley, K. S. Murray, Y. Lan, W. Wernsdorfer, G. Rajaraman and M. Shanmugam, *Inorg. Chem.*, 2016, **55**, 9564–9578.
31 C. Villa-Pérez, I. Oyarzabal, G. A. Echeverría, G. C. Valencia-Uribe, J. M. Seco and D. B. Soria, *Eur. J. Inorg. Chem.*, 2016, **2016**, 4835–4841.
32 J. Walsh, G. Bowling, A.-M. Ariciu, N. Jailani, N. Chilton, P. Waddell, D. Collison, F. Tuna and L. Higham, *Magnetochemistry*, 2016, **2**, 23.
33 D. Valigura, C. Rajnák, J. Moncol, J. Titiš and R. Boča, *Dalton Trans.*, 2017, **46**, 10950–10956.
34 C. Rajnák, J. Titiš, J. Moncol', F. Renz and R. Boča, *Eur. J. Inorg. Chem.*, 2017, **2017**, 1520–1525.
35 F. Varga, C. Rajnak, J. Titis, J. Moncol and R. Boca, *Dalton Trans.*, 2017, **46**, 4148–4151.
36 S. Gómez-Coca, A. Urtizberea, E. Cremades, P. J. Alonso, A. Camón, E. Ruiz and F. Luis, *Nat. Commun.*, 2014, **5**, 4300.
37 Y. Peng, V. Mereacre, C. E. Anson, Y. Zhang, T. Bodenstein, K. Fink and A. K. Powell, *Inorg. Chem.*, 2017, **56**, 6056–6066.
38 J. Sanmartín-Matalobos, C. Portela-García, M. Fondo and A. M. García-Deibe, *Cryst. Growth Des.*, 2015, **15**, 4318–4323.
39 J. K. McCusker, A. L. Rheingold and D. N. Hendrickson, *Inorg. Chem.*, 1996, **35**, 2100–2112.
40 M. Marchivie, P. Guionneau, J. F. Létard and D. Chasseau, *Acta Crystallogr. Sect. B Struct. Sci.*, 2005, **61**, 25–8.
41 S. Alvarez, *Chem. Rev.*, 2015, **115**, 13447–13483.
42 A. M. García-Deibe, C. Portela-García, M. Fondo, A. J. Mota and J. Sanmartín-Matalobos, *Chem. Commun.*, 2012, **48**, 9915.
43 N. F. Chilton, R. P. Anderson, L. D. Turner, A. Soncini and K. S. Murray, *J. Comput. Chem.*, 2013, **34**, 1164–1175.
44 F. Neese, *WIREs Comput. Mol. Sci.*, 2012, **2**, 73–78.
45 G. Karlström, R. Lindh, P.-Å. Malmqvist, B. O. Roos, U. Ryde, V. Veryazov, P. O. Widmark, M. Cossi, B. Schimmelpfennig, P. Neogrady and L. Seijo, in *Computational Materials Science*, Elsevier, 2003, vol. 28, pp. 222–239.
46 V. Veryazov, P.-O. Widmark, L. Serrano-Andrés, R. Lindh and B. O. Roos, *Int. J. Quantum Chem.*, 2004, **100**, 626–635.
47 F. Aquilante, L. De Vico, N. Ferré, G. Ghigo, P.-Å. Malmqvist, P. Neogrády, T. B. Pedersen, M. Pitoňák, M. Reiher, B. O. Roos, L. Serrano-Andrés, M. Urban, V. Veryazov and R. Lindh, *J. Comput. Chem.*, 2010, **31**, 224–247.
48 S. Gómez-Coca, E. Cremades, N. Aliaga-Alcalde and E. Ruiz, *J. Am. Chem. Soc.*, 2013, **135**, 7010.
49 M. Atanasov, D. Ganyushin, K. Sivalingam and F. Neese, in *Molecular Electronic Structures of Transition Metal Complexes II. Structure and Bonding*, eds. D. M. P. Mingos, P. Day and J. P. Dahl, Springer, Berlin, 2012, pp. 149–220.
50 M. Atanasov, D. Aravena, E. Suturina, E. Bill, D. Maganas and F. Neese, *Coord. Chem. Rev.*, 2015, **289–290**, 177–214.
51 E. A. Buvaylo, V. N. Kokozay, O. Y. Vassilyeva, B. W. Skelton, A. Ozarowski, J. Titiš, B. Vranovičová and R. Boča, *Inorg. Chem.*, 2017, **56**, 6999–7009.
52 M. A. Palacios, J. Nehrkorn, E. A. Suturina, E. Ruiz, S. Gómez-Coca, K. Holldack, A. Schnegg, J. Krzystek, J. M. Moreno and E. Colacio, *Chem. Eur. J.*, 2017, **23**, 11649–11661.
53 *Bruker APEXII*, Bruker AXS Inc., Madison, USA, 2005.
54 *SADABS and SAINT*, Bruker AXS Inc., Madison, USA, 2013.
55 Rigaku, *Rigaku XRD*, Rigaku Corporation, Tokyo, Japan, 1996.
56 G. M. Sheldrick, *Acta Crystallogr. Sect. A Found. Crystallogr.*, 2015, **71**, 3–8.
57 G. M. Sheldrick, *Acta Crystallogr. Sect. C Struct. Chem.*, 2015, **71**, 3–8.
58 L. J. Bourhis, O. V. Dolomanov, R. J. Gildea, J. A. K. Howard and H. Puschmann, *Acta Cryst.*, 2015, **A71**, 59–75.
59 O. V. Dolomanov, L. J. Bourhis, R. J. Gildea, J. A. K. Howard and H. Puschmann, *J. Appl. Cryst.*, 2009, **42**, 339–42.
60 L. F. Chibotaru, L. Ungur and A. Soncini, *Angew. Chemie Int. Ed.*, 2008, **47**, 4126–4129.
61 L. F. Chibotaru, L. Ungur, C. Aronica, H. Elmoll, G. Pilet and D. Luneau, *J. Am. Chem. Soc.*, 2008, **130**, 12445–12455.
62 B. O. Roos, V. Veryazov and P.-O. Widmark, *Theor. Chem. Acc.*, 2004, **111**, 345–351.
63 B. O. Roos, R. Lindh, P.-Å. Malmqvist, V. Veryazov and P.-O. Widmark, *J. Phys. Chem. A*, 2004, **108**, 2851–2858.
64 B. O. Roos, R. Lindh, P.-Å. Malmqvist, V. Veryazov and P.-O. Widmark, *J. Phys. Chem. A*, 2005, **109**, 6575–6579.
65 B. O. Roos, R. Lindh, P.-Å. Malmqvist, V. Veryazov and P.-O. Widmark, *Chem. Phys. Lett.*, 2005, **409**, 295–299.
66 C. Angeli, R. Cimiraglia, S. Evangelisti, T. Leininger and J.-P. Malrieu, *J. Chem. Phys.*, 2001, **114**, 10252–10264.
67 C. Angeli, R. Cimiraglia and J.-P. Malrieu, *Chem. Phys. Lett.*, 2001, **350**, 297–305.
68 C. Angeli, R. Cimiraglia and J.-P. Malrieu, *J. Chem. Phys.*, 2002, **117**, 9138–9153.
69 F. Weigend and R. Ahlrichs, *Phys. Chem. Chem. Phys.*, 2005, **7**, 3297.
70 F. Weigend, *Phys. Chem. Chem. Phys.*, 2006, **8**, 1057.

 